

- <sup>62</sup>V. A. Tyagai, V. N. Bondarenko, and O. V. Snitko, *Fiz. Tekh. Poluprovodn.* **5**, 1038 (1971) [*Sov. Phys.-Semicond.* **5**, 920 (1971)]; F. Evangelisti, A. Frova, and J. U. Fischbach, *Phys. Rev. Lett.* **29**, 1001 (1972).
- <sup>63</sup>L. V. Keldysh, O. V. Konstantinov, and V. I. Perel', *Fiz. Tekh. Poluprovodn.* **3**, 1042 (1969) [*Sov. Phys.-Semicond.* **3**, 876 (1970)].
- <sup>64</sup>P. Lawaetz, *Phys. Rev. B* **4**, 3460 (1971).
- <sup>65</sup>D. F. Blossey, *Phys. Rev. B* **2**, 3976 (1970); *Phys. Rev. B* **3**, 1382 (1971).
- <sup>66</sup>J. D. Dow and D. Redfield, *Phys. Rev. B* **1**, 3358 (1970).
- <sup>67</sup>F. C. Weinstein, J. D. Dow, and B. Y. Lao, *Phys. Rev. B* **4**, 3502 (1971).
- <sup>68</sup>A more accurate line-shape analysis of the WDR measurements of Ref. 28 has been performed [D. D. Sell (private communication)], and yields an energy of  $1855 \pm 2$  meV for the  $n = 1$  exciton at the  $E_0 + \Delta_0$  transition in GaAs at 2°K. This value should replace the energy,  $1850 \pm 5$  meV, reported in Ref. 28.
- <sup>69</sup>F. H. Pollack, C. W. Higginbotham, and M. Cardona, *J. Phys. Soc. Jap. Suppl.* **21**, 20 (1966).
- <sup>70</sup>M. L. Cohen and T. K. Bergstresser, *Phys. Rev.* **141**, 789 (1966).
- <sup>71</sup>F. Herman, R. L. Kortum, C. D. Kuglin, J. P. Van Dyke, and S. Skillman, in *Methods of Computational Physics*, edited by B. Alder, S. Fernbach, and M. Rotenberg (Academic, New York, 1968), p. 193. See Table V.
- <sup>72</sup>I. B. Ortenberger and W. E. Rudge (unpublished).
- <sup>73</sup>M. Cardona and D. L. Greenaway, *Phys. Rev.* **125**, 1291 (1962).
- <sup>74</sup>B. O. Seraphin and N. Bottka, *Phys. Rev.* **145**, 628 (1966).
- <sup>75</sup>D. E. Aspnes (unpublished).
- <sup>76</sup>J. E. Fischer, in Ref. 6, p. 427.
- <sup>77</sup>D. E. Aspnes, *Phys. Rev.* **153**, 972 (1967). See also the listing of the functional forms in Tables II and III in D. E. Aspnes and N. Bottka, Ref. 3, p. 457.
- <sup>78</sup>J. Grover, S. Koeppen, and P. Handler, *Phys. Rev. B* **4**, 2830 (1971).
- <sup>79</sup>See Fig. 12 of Ref. 67.
- <sup>80</sup>E. O. Kane, *J. Phys. Chem. Solids* **1**, 249 (1956).
- <sup>81</sup>D. E. Aspnes, *Phys. Rev.* **147**, 554 (1966).
- <sup>82</sup>J. E. Fischer and N. Bottka, *Phys. Rev. Lett.* **24**, 1292 (1970).
- <sup>83</sup>E. Schmidt, *Phys. Status Solidi B* **45**, K39 (1971).
- <sup>84</sup>G. G. Wepfer, T. C. Collins, and R. N. Euwema, *Phys. Rev. B* **4**, 1296 (1971).
- <sup>85</sup>D. E. Aspnes and A. A. Studna, *Solid State Commun.* **11**, 1375 (1972).
- <sup>86</sup>D. E. Aspnes, K. E. Benson, and A. A. Studna (unpublished).
- <sup>87</sup>D. E. Aspnes, P. Handler, and D. F. Blossey, *Phys. Rev.* **166**, 921 (1968).
- <sup>88</sup>J. E. Rowe and D. E. Aspnes, *Phys. Rev. Lett.* **25**, 162 (1970).

## Lattice Thermal Conductivity of Mercury Selenide\*

Charles R. Whitsett, Donald A. Nelson, J. G. Broerman, and E. C. Paxhia†

McDonnell Douglas Research Laboratories, McDonnell Douglas Corporation, St. Louis, Missouri 63166

(Received 8 September 1972)

The lattice thermal conductivity between 1.7 and 270 K is reported for single crystals of mercury selenide having conduction electron concentrations from  $2.1 \times 10^{17}$  to  $6.7 \times 10^{18}$  cm<sup>-3</sup>. The most striking feature of the data for HgSe is the pronounced depression of the magnitude of the thermal conductivity between 4 and 30 K, and this is attributed to the Wagner mechanism for third-order phonon-annihilation resonance scattering of phonons. The data were analyzed by using the Callaway formalism to determine the relaxation times for phonon scattering by normal and umklapp processes, point defects, resonance modes, crystal boundaries, and conduction electrons. The resonance dip in thermal conductivity was observed in variously prepared HgSe samples, including specially purified and vapor-deposited crystals. Addition of sulfur impurity to HgSe apparently enhanced the resonance scattering, but because sulfur considerably altered the normal and umklapp scattering it could not be concluded if substitutional sulfur atoms were the resonantly scattering centers or if they only indirectly affected the resonance. The ionized defects in HgSe, in concentrations corresponding to as many as  $3 \times 10^{18}$  conduction electrons/cm<sup>3</sup>, acted as point Rayleigh scattering centers, but there was no increase in the Rayleigh scattering as the electron concentration was increased above  $3 \times 10^{18}$  cm<sup>-3</sup>.

### I. INTRODUCTION

Mercury selenide (HgSe) is a II-VI compound with the same cubic zinc-blende structure as the well-known III-V semiconducting compounds.<sup>1</sup> However, like  $\alpha$ -Sn<sup>2</sup> and HgTe,<sup>3</sup> it is a zero-gap semiconductor or perfect semimetal by virtue of a symmetry-induced degeneracy of the valence-band maximum and conduction-band minimum.<sup>4-6</sup> Because of this peculiar band structure, the zero-gap

semiconductors display a number of anomalous features in their dielectric,<sup>7-9</sup> transport,<sup>10,11</sup> and lattice dynamic behavior.<sup>12</sup> To understand the phonon interactions and defect properties of these structures, we have investigated the thermal-transport properties of HgSe.

We report here the thermal conductivity between 1.7 and 270 K of HgSe single crystals prepared in different ways and subjected to various annealing procedures. The low-temperature thermal con-

ductivity of HgSe has been reported previously by Aliev, Korenblit, and Shalyt<sup>13</sup> (AKS). However, our results differ in a number of ways which will be discussed. The most striking feature of our results is a pronounced dip in the thermal conductivity between 4 and 30 K, which can be interpreted only as the resonant scattering of acoustic phonons in a third-order process involving localized modes of the defect lattice. We analyze this process in detail and also present results on the Rayleigh (point-defect), crystal-boundary, normal, umklapp, and electron-phonon scattering processes.

HgSe invariably grows as an *n*-type material with an ionized-defect concentration of  $(3-6) \times 10^{18} \text{ cm}^{-3}$ , although the concentration of ionized defects can be changed by various annealing procedures. The defects are probably defects native to the lattice rather than chemical impurity defects. We analyze in detail the relation between the ionized-defect densities (as reflected in the Rayleigh scattering of phonons) and the conduction-electron densities. We also find evidence for a remanent neutral-defect density of about the same value as that which has been invoked to explain the anomalous electron mobility in  $\alpha$ -Sn.<sup>11</sup>

In previous literature,<sup>14-18</sup> estimates of the room-temperature lattice thermal conductivity ranged from 0.005 to 0.021  $\text{W cm}^{-1} \text{K}^{-1}$ . One reason for the spread of values is that at room temperature the electronic contribution to the total thermal conductivity is substantial but difficult to determine with precision. AKS endeavored to determine the electronic thermal conductivity in HgSe at temperatures between 30 and 200 K, and Smirnov and Aliev<sup>19</sup> analyzed the electronic thermal conductivity between 80 and 440 K. Their results will be discussed later in connection with the method used here to separate the electronic and lattice contributions to the total thermal conductivity.

## II. EXPERIMENTAL PROCEDURE

Except for one vapor-grown crystal, the HgSe compound was prepared and single crystals were grown by the method previously reported by Whitsett and Nelson.<sup>20</sup> Single-crystal samples were cut to size and mechanically polished, the final polish being obtained with 0.05- $\mu\text{m}$ -diam particle alumina abrasive. The as-grown crystals of HgSe had electron concentrations of about  $4.8 \times 10^{18} \text{ cm}^{-3}$  at room temperature and below. Spectrographic analyses of the HgSe crystals showed the major metallic impurities to be Cu (0.1-0.7 ppm), Mg (0.5-0.1 ppm), and Si (0-9 ppm). Chemical analyses indicated that Te impurity, if present, was less than 10 ppm and that S was present in concentrations possibly as large as 20-30 ppm by weight.

The absolute, steady-state, longitudinal-heat-flow method was used to determine the thermal conductivity. With this method a temperature gradient  $dT/dx$  is established along the length of the sample by introducing a heat flow  $W$  at one end and extracting it at the other end. If no heat is lost through the sides of the sample, the thermal conductivity is

$$\kappa = \frac{W}{\mathcal{A}} \left( \frac{dT}{dx} \right)^{-1}, \quad (1)$$

where  $\mathcal{A}$  is the cross-sectional area of the sample. The apparatus and techniques used were as described previously.<sup>21</sup>

Radiation-loss corrections to the measured thermal conductivity were made based upon calculations which were believed to be accurate to within a factor of 2. The maximum possible error in the measurement of total thermal conductivity was estimated to be  $\pm 4.5\%$  at temperatures lower than 100 K,  $\pm 5.5\%$  at 125 K, and  $\pm 9.0\%$  at 155 K. The increase in the error with temperature is due primarily to the correspondingly increasing importance of radiation loss.

The preparation details and annealing histories of the samples used in this study are summarized in Table I. The electron concentration  $n$  was computed by assuming  $n = -1/Re$ , where  $R$  is the Hall coefficient and  $e$  is the magnitude of the charge of an electron. In Table II are compiled the electron concentrations at 4.2 K and the electrical conductivities at 4.2, 77.3, and 300 K. In Fig. 1 are plotted the electrical conductivities as functions of temperature for all of the samples reported upon here. The total thermal conductivity as a function of temperature for a number of undoped HgSe single crystals is shown in Figs. 2-4. The data points

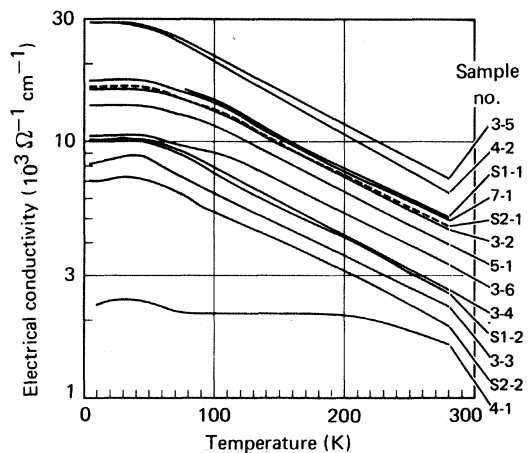


FIG. 1. Electrical conductivity as function of temperature for single-crystal HgSe samples used in thermal-conductivity study.

TABLE I. Thermal histories and cross-sectional dimensions of the HgSe thermal-conductivity samples. As-grown samples were cooled slowly from the 799 °C melting temperature. Lengths of samples were between 2 and 5 cm.

HgSe sample No.	Thermal history (and cross-sectional dimensions)
3-2	As-grown (0.55 × 0.55 cm)
3-3	HgSe 3-2 subsequently annealed in vacuum at 240 °C for 12 h, 210 °C for 100 h, 190 °C for 12 h, and 180 °C for 5 h (0.55 × 0.55 cm)
3-4	HgSe 3-3 subsequently annealed in Se vapor at 200 °C for 36 h (0.55 × 0.55 cm)
3-5	HgSe 3-4 subsequently annealed in Hg vapor at 235 °C for 48 h and 255 °C for 24 h (0.55 × 0.55 cm)
3-6	HgSe 3-5 subsequently annealed in Se vapor at 280 °C for 48 h (0.55 × 0.55 cm)
4-1	After growth, annealed in vacuum at 257 °C for 24 h and 208 °C for 96 h (0.58 × 0.58 cm)
4-2	HgSe 4-1 subsequently annealed in Hg vapor at 235 °C for 48 h and 255 °C for 24 h (0.58 × 0.58 cm)
5-1	As-grown (0.57 × 0.57 cm)
6-1	Starting materials triply distilled in vacuum; as-grown (0.63 × 0.63 cm)
7-1	Excess Hg in melt, 6 wt.%; as-grown (0.41 × 0.27 cm)
S1-1	Sulfur added to melt, $5 \times 10^{19}$ atoms/cm <sup>3</sup> ; as-grown (0.57 × 0.57 cm)
S1-2	HgSe S1-1 subsequently annealed in vacuum at 257 °C for 24 h, 235 °C for 24 h, and 210 °C for 72 h (0.55 × 0.55 cm)
S2-1	Sulfur added to melt, $5 \times 10^{20}$ atoms/cm <sup>3</sup> ; as-grown (0.51 × 0.50 cm)
S2-2	HgSe S2-1 subsequently annealed in vacuum at 258 °C for 18 h, 235 °C for 46 h, and 210 °C for 25 h (0.47 × 0.46 cm)

shown have been corrected for radiation-loss errors.

### III. LATTICE THERMAL CONDUCTIVITY

The qualitative features of the data shown in Figs. 2-4 may be explained by assuming that six phonon scattering mechanisms limit the lattice contribution to the total thermal conductivity. At the lowest temperatures the thermal conductivity falls with decreasing temperatures because of the scattering of phonons by the crystal boundaries and by conduction electrons. Near 4 K the thermal conductivity is a maximum and limited primarily by the Rayleigh scattering of phonons by point de-

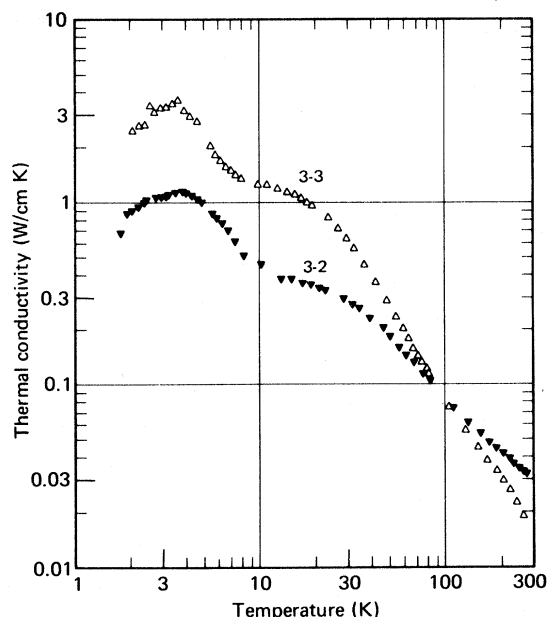


FIG. 2. Total thermal conductivity as function of temperature for HgSe 3-2 ( $\blacktriangledown$ ) and HgSe 3-3 ( $\Delta$ ). HgSe 3-2 was as-grown and had  $3.0 \times 10^{18}$  electrons/cm<sup>3</sup>; HgSe 3-3 was vacuum annealed and had  $5.7 \times 10^{17}$  electrons/cm<sup>3</sup> at 4.2 K.

fects. Between 4 and 30 K, the thermal conductivity exhibits a pronounced dip which we interpret to be due to the scattering of phonons by a resonance process. As the temperature increases from 30 K to room temperature, the lattice thermal conductivity is limited mainly by umklapp and normal processes.

The Callaway theoretical model<sup>22</sup> was used to

TABLE II. Conduction-electron concentration  $n$ , electrical conductivity  $\sigma$ , electron effective-mass ratio  $m^*/m_e$ , and electron-phonon cutoff temperature  $\Theta_k = 2\nu\hbar(3\pi^2/n)^{1/3}/K$  of HgSe thermal-conductivity samples.

HgSe sample No.	$10^{-18}n$	$10^{-3}\sigma$			$m^*/m_e$	$\Theta_k$
	(4.2 K) (cm <sup>-3</sup> )	4.2 K	77 K	300 K		
3-2	3.0	16	12	4.0	0.061	13.2
3-3	0.57	8.5	7.2	2.0	0.041	7.6
3-4	0.80	10	9.1	2.3	0.044	8.5
3-5	6.7	29	25	6.4	0.075	17.2
3-6	1.3	10	9.6	3.0	0.050	10.0
4-1	0.21	2.4	2.1	1.4	0.035	5.4
4-2	5.3	29	24	5.5	0.071	15.9
5-1	2.2	13	12	3.8	0.056	12.0
S1-1	4.2		16	4.6	0.066	14.7
S1-2	0.83	10	8.7	2.4	0.045	8.6
S2-1	4.0	16	15	4.2	0.065	14.5
S2-2	0.49	7.0	6.2	1.6	0.040	7.2

<sup>a</sup>Calculated from Eq. (18).

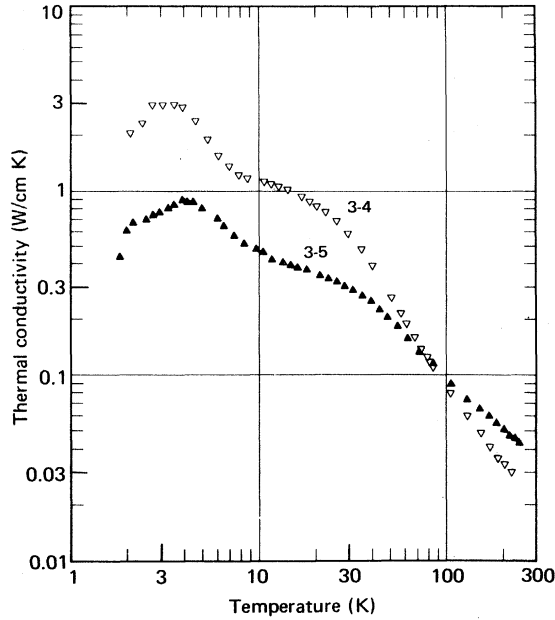


FIG. 3. Total thermal conductivity as function of temperature for HgSe 3-4 ( $\nabla$ ) and HgSe 3-5 ( $\blacktriangle$ ). HgSe 3-4 was Se-vapor annealed and had  $8.0 \times 10^{17}$  electrons/cm<sup>3</sup> at 4.2 K; HgSe 3-5 was Hg-vapor annealed and had  $6.7 \times 10^{18}$  electrons/cm<sup>3</sup>.

analyze the data. This model gives for the lattice thermal conductivity

$$\kappa_L = (K/2\pi^2v) (I_1 + \beta I_2), \quad (2)$$

where

$$I_1 = \int_0^{K\Theta/\hbar} \tau_c \left( \frac{\hbar\omega}{KT} \right)^2 \frac{e^{\hbar\omega/KT}}{(e^{\hbar\omega/KT} - 1)^2} \omega^2 d\omega, \quad (3)$$

$$I_2 = \int_0^{K\Theta/\hbar} \frac{\tau_c}{\tau_N} \left( \frac{\hbar\omega}{KT} \right)^2 \frac{e^{\hbar\omega/KT}}{(e^{\hbar\omega/KT} - 1)^2} \omega^2 d\omega, \quad (4)$$

and

$$\beta = I_2 / \int_0^{K\Theta/\hbar} \frac{1}{\tau_N} \left( 1 - \frac{\tau_c}{\tau_N} \right) \left( \frac{\hbar\omega}{KT} \right)^2 \frac{e^{\hbar\omega/KT}}{(e^{\hbar\omega/KT} - 1)^2} \omega^2 d\omega \quad (5)$$

In these equations,  $\tau_N$  is the phonon relaxation time for normal momentum-conserving processes, and  $\tau_c$  is the resultant relaxation time for all phonon scattering processes. Also,  $K$  is the Boltzmann constant,  $\Theta$  is the Debye temperature,  $\hbar$  is Planck's constant divided by  $2\pi$ ,  $v$  is the average speed of sound, and  $\omega = 2\pi\nu$ , where  $\nu$  is the phonon frequency. In terms of the phonon wave number  $q$ , the relationship for  $\omega$  is  $\omega = vq$ .

The phonon relaxation times for normal processes, umklapp processes, Rayleigh scattering, boundary scattering, resonance scattering, and electron-phonon scattering will be denoted, respectively, by  $\tau_N$ ,  $\tau_U$ ,  $\tau_A$ ,  $\tau_B$ ,  $\tau_R$ , and  $\tau_k$ . The sum

of the inverses of these relaxation times will be taken to give the inverse of  $\tau_c$ , the relaxation time resulting from the combined effect of all scattering processes. That is,

$$\tau_c^{-1} = \tau_N^{-1} + \tau_U^{-1} + \tau_A^{-1} + \tau_B^{-1} + \tau_R^{-1} + \tau_k^{-1}. \quad (6)$$

For the inverse relaxation time for normal processes, the expression of Callaway<sup>22</sup> was used:  $\tau_N^{-1} = B_2 T^3 \omega^2$ . For the inverse relaxation time for umklapp processes, we departed from the formulation of Callaway (who used  $\tau_U^{-1} = B_1 T^3 \omega^2$ ) and followed Slack and Galginaitis<sup>23</sup> who used

$$\tau_U^{-1} = B_1' T \omega^2 e^{-\Theta/aT}, \quad (7)$$

where  $a$  is a constant of the order of unity. The form of Eq. (7) gives a temperature dependence for the thermal conductivity which closely matches that obtained experimentally. Slack and Galginaitis determined the form of Eq. (7) empirically and further derived

$$B_1' \approx \hbar\gamma^2 / Mv^2\Theta, \quad (8)$$

where  $M$  is the average atomic mass and  $\gamma$  is the Grüneisen constant (here assumed to be 2.0). For HgSe, Eq. (8) gives  $B_1' = 3.21 \times 10^{-18}$  sec K<sup>-1</sup>.

For Rayleigh scattering by point defects, the inverse relaxation time was taken to be  $\tau_A^{-1} = A\omega^4$ . The parameter  $A$  is the sum of at least two terms:  $A_{\text{isot}}$  for the scattering caused by the natural distribution of isotopes of the elements in the com-

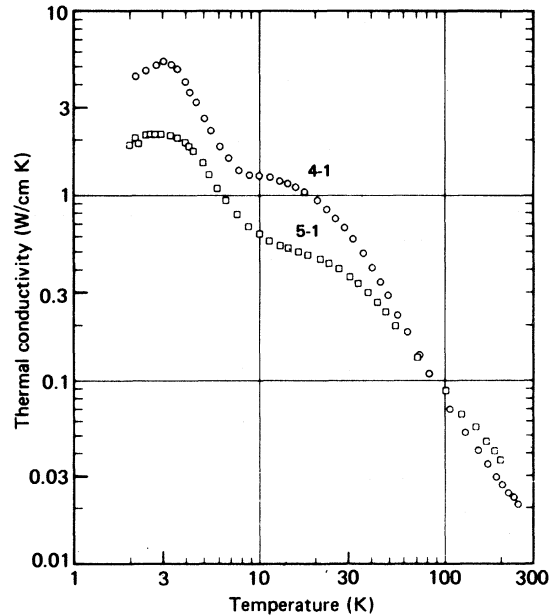


FIG. 4. Total thermal conductivity as function of temperature for HgSe 4-1 ( $\circ$ ) and HgSe 5-1 ( $\square$ ). HgSe 4-1 was vacuum annealed and had  $2.1 \times 10^{17}$  electrons/cm<sup>3</sup> at 4.2 K; HgSe 5-1 was as-grown and had  $2.2 \times 10^{18}$  electrons/cm<sup>3</sup>.

pound, and  $A_{\text{imp}}$  for the scattering by point defects such as Hg and Se vacancies and interstitials.

The isotope scattering may be calculated by using the result of Klemens<sup>24</sup> for an isolated substitutional atom with mass difference  $\Delta M$ ,

$$\frac{1}{\tau_{\text{isot}}} = A_{\text{isot}}\omega^4 = \frac{a_0^3}{4\pi v^3 G} \left(\frac{\Delta M}{M}\right)^2 \omega^4, \quad (9)$$

where  $a_0^3$  is the unit cell volume,  $G$  is the number of unit cells in the crystal, and  $M$  is the mass per unit cell. For each atomic species, we define the quantities  $\bar{m} = \sum f_i m_i$  and  $\Gamma = \sum f_i [(m_i - \bar{m})/\bar{m}]^2$ , where  $m_i$  is the mass of the  $i$ th isotope and  $f_i$  is the fractional natural abundance of the isotope. Equation (9), summed over all unit cells, becomes

$$\frac{1}{\tau_{\text{isot}}} = \frac{a_0^3}{4\pi v^3 G} \sum_{i=1}^G \left(\frac{\Delta M_i}{M}\right)^2 \omega^4, \quad (10)$$

where  $M$  is the average value for the sum of the atomic masses in a unit cell and  $\Delta M_i$  is the deviation from  $M$  of the mass in the  $i$ th cell resulting from isotopic mass variations. In the case of HgSe, for which  $a_0 = 6.085 \text{ \AA}$ ,<sup>25</sup> Eq. (10) is

$$\begin{aligned} \frac{1}{\tau_{\text{isot}}} &= \frac{a_0^3}{16\pi^3} \left(\frac{1}{\bar{m}_{\text{Hg}} + \bar{m}_{\text{Se}}}\right)^2 [(\bar{m}_{\text{Hg}})^2 \Gamma_{\text{Hg}} + (\bar{m}_{\text{Se}})^2 \Gamma_{\text{Se}}] \omega^4 \\ &= (4.29 \times 10^{-44} \text{ sec}^3) \omega^4. \end{aligned} \quad (11)$$

Klemens<sup>24</sup> calculated the inverse relaxation time for substitutional atom or vacancy scattering in a monatomic crystal to be

$$\frac{1}{\tau_{\text{imp}}} = A_{\text{imp}}\omega^4 = \frac{3V_0^2}{\pi v^3} \sum_i N_i S_i^2 \omega^4, \quad (12)$$

where  $N_i$  is the concentration and  $S_i$  is the scattering factor of the  $i$ th type of defect, and  $V_0$  is the atomic volume. In the case of diatomic HgSe,  $V_0$  is the primitive unit cell volume:  $V_0 = \frac{1}{4}a_0^3$ . The scattering factor  $S_i$  depends in detail upon the binding forces of the defect as well as the mass change, but it usually has a value near unity. Klemens<sup>24</sup> calculated  $S_i$  for a number of cases of substitutional impurities or vacancies in alkali halides and obtained values ranging from 0.5 to 2.1. For HgSe,

$$\frac{1}{\tau_{\text{imp}}} = (4.08 \times 10^{-61} \text{ cm}^3) \left(\sum_i N_i S_i^2\right) \omega^4. \quad (13)$$

The inverse relaxation time for scattering of phonons by the crystal boundaries was taken to be

$$\tau_B^{-1} = v/F(1.12\alpha^{1/2}), \quad (14)$$

where  $\alpha$  is the cross-sectional area of the sample and  $F$  is related to the fraction  $f$  of phonons which are diffusely scattered at the boundaries, according to  $F = (2-f)/f$ . This formula for  $\tau_B^{-1}$ , based upon the works of Casimir<sup>26</sup> and of Berman, Simon, and Ziman,<sup>27</sup> makes no allowance for finite sample length as discussed by Berman, Foster,

and Ziman.<sup>28</sup>

For the HgSe crystals with electron concentrations greater than  $1 \times 10^{18} \text{ cm}^{-3}$ , the thermal conductivity below 4 K is too low to be satisfactorily explained as being limited only by the boundary scattering of phonons. It is apparent that the scattering of phonons by conduction electrons also contributes to limiting the magnitude of the low-temperature thermal conductivity. For a simple cubic material with a spherically symmetric conduction band, only longitudinal phonons should be scattered by electrons, and the inverse relaxation time for the process is<sup>29</sup>

$$\tau_k^{-1} = \begin{cases} D(m^*/m_e)^2 \omega & (\omega \leq 2vk_F) \\ 0 & (\omega > 2vk_F) \end{cases}, \quad (15)$$

where

$$D = (m_e)^2 (E_{\text{def}})^2 / 2\pi\rho\hbar^3 v, \quad (16)$$

$m^*$  is the electron effective mass in HgSe,  $m_e$  is the free-electron mass,  $E_{\text{def}}$  is the lattice deformation potential,  $\rho$  is the crystal density, and  $k_F$  is the radius of the Fermi surface. For face-centered-cubic HgSe, because of the  $p^{3/2}$ -like symmetry of the conduction-band wave functions, both transverse and longitudinal phonons can interact with electrons and here are assumed to have the same relaxation times. With  $\tau_k^{-1}$  contributing to the sum  $\tau_c^{-1}$ , the integrals in Eqs. (3)–(5) each become the sum of two integrals, one with the limits zero and  $K\Theta_k/\hbar$  and the other with the limits  $K\Theta_k/\hbar$  and  $K\Theta/\hbar$ , where  $\Theta_k = 2v\hbar k_F/K$ . As a function of electron concentration  $n$ , the Fermi-surface radius is  $k_F = (3\pi^2 n)^{1/3}$ , and

$$\Theta_k = 2v\hbar(3\pi^2 n)^{1/3}/K. \quad (17)$$

The dependence upon electron concentration of the electron effective mass in HgSe is given by the following formula which is based upon the theory of Kane<sup>30</sup>:

$$m^* = m_e \left[ 1 + \frac{4m_e P^2}{3\hbar^2} \left( E_G^2 + \frac{8k_F^2 P^2}{3} \right)^{-1/2} \right]^{-1}. \quad (18)$$

In Eq. (18),  $E_G$  is the  $\Gamma_6-\Gamma_8$  band gap at the center origin of the Brillouin zone, and  $P$  is the interband momentum matrix element. The values 0.24 eV for  $E_G$  and  $7.1 \times 10^{-8} \text{ eV cm}$  for  $P$  were used, based upon Shubnikov-de Haas measurements on HgSe.<sup>31</sup>

A defect introduced into a lattice, in addition to providing a center for ordinary Rayleigh scattering, also produces changes in the normal modes of the lattice itself. In particular, it introduces a localized part in the wave functions of the acoustic phonons. For most frequencies the plane-wave part is dominant, so that a description in terms of phonons still is valid. However, there may occur a small interval about a resonant frequency  $\omega_s$  for which the localized part dominates, and this intro-

duces the possibility of new scattering processes between phonons characterized by a wave vector  $\vec{q}$  and polarization  $\lambda$  and localized modes characterized by a quantum number  $s$ . For a simple substitutional defect, which introduces no new normal modes, the new processes are of third order,

$$(\vec{q}\lambda) + (\vec{q}'\lambda') = (s), \quad (19a)$$

$$\omega(\vec{q}\lambda) + \omega(\vec{q}'\lambda') = \omega_s \quad (19b)$$

and

$$(\vec{q}\lambda) + (s) = (\vec{q}'\lambda'), \quad (20a)$$

$$\omega(\vec{q}\lambda) + \omega_s = \omega(\vec{q}'\lambda'), \quad (20b)$$

while the second-order process

$$(\vec{q}\lambda) = (s) \quad (21)$$

is forbidden by energy conservation. If the defect is complex, i. e., has internal modes, then the second-order process is also allowed.

Wagner<sup>32</sup> calculated the relaxation times for the third-order resonant processes. He found that the process of Eqs. (20) is important only at high temperatures. The relaxation time for the process of Eqs. (19) is given by

$$\tau_R^{-1} = \frac{9}{16} \frac{\pi^2}{\rho} \frac{\hbar\gamma^2}{v^2} \frac{\omega_s}{\omega_\alpha} N g(\omega) f(\omega, T) h(\omega), \quad (22a)$$

$$g(\omega) = \left(1 + 4 \frac{\omega_s}{\omega_\alpha}\right) \ln \left[ \frac{\omega_\alpha}{\omega_s} \frac{\omega}{\omega_s} \left(1 - \frac{\omega}{\omega_s}\right) + 1 \right] - 4 \frac{\omega}{\omega_s} \left(1 - \frac{\omega}{\omega_s}\right), \quad (22b)$$

$$f(\omega, T) = \frac{(\omega_s - \omega)^2 e^{(\omega_s - \omega)\hbar/KT} (e^{\hbar\omega/KT} - 1)}{(e^{\hbar\omega_s/KT} - 1) (e^{(\omega_s - \omega)\hbar/KT} - 1)}, \quad (22c)$$

$$h(\omega) = \begin{cases} \theta(\omega - \omega_s) & (\omega_s \leq \omega_D) \\ \theta(\omega_s - \omega_D - \omega) \theta(\omega - \omega_D) & (\omega_s > \omega_D) \end{cases}; \quad (22d)$$

$$\theta(y) = \begin{cases} 1 & (y \leq 0) \\ 0 & (y > 0) \end{cases}.$$

In these expressions,  $\gamma$  is the Grüneisen constant,  $N$  is the product of the concentration of resonant scattering centers by the number of modes per center,  $\omega_D$  is the Debye frequency ( $\omega_D = \Theta/\hbar$ ),  $\omega_s$  is the average resonant frequency of a scattering center, and  $\omega_\alpha = \alpha_c$ , where  $\alpha_c^{-1}$  is the effective "radius" of a scattering center.

The relaxation time given by Wagner's resonance scattering model has the temperature dependence necessary to fit the data. A resonance scattering cross section is required which is sharply cut off on the low-temperature side. For this reason, a mechanism such as that proposed by Krumhansl<sup>33</sup> for vacancy scattering or the process of Eq. (21) could not fit these data. As an alternative to resonance scattering, the method of Holland<sup>34</sup> for con-

sidering separately the contributions of longitudinal and transverse phonons was tried, but the data could not be fit at all well in this way without including resonance scattering.

The model for the lattice thermal conductivity of HgSe which we have described is admittedly defective. Lumping together the effects of the transverse and longitudinal phonons cannot be justified, and the assumption of the Debye-phonon dispersion relation with a temperature-independent cutoff frequency is a drastic oversimplification. However, there simply is not enough known about the acoustic-phonon dispersion characteristics of HgSe to justify a more sophisticated model with an accompanying proliferation of parameters not now known.

Of the scattering parameters included in the thermal-conductivity model, the set  $A$ ,  $F$ ,  $\omega_s$ ,  $N$ , and  $D$  is most influential below 30 K, and at these lower temperatures the model is insensitive to the value of the Debye cutoff frequency. Thus, by fitting the data, reasonably reliable values for these parameters should be obtained. Above 30 K, the normal and umklapp scattering processes are the more influential, and the values obtained for the parameters  $B'_1$ ,  $B_2$ , and  $a$  are affected strongly by the value used for the Debye cutoff frequency.

#### IV. ELECTRONIC THERMAL CONDUCTIVITY

If the only thermal conduction were by the lattice, then the thermal conductivity should be about the same for all samples above 100 K. However, beginning near the temperature of liquid nitrogen, the conduction electrons carry an increasingly significant portion of heat as the temperature is increased. The electronic thermal conductivity is larger for larger electron concentrations. At temperatures below 100 K, the samples with the larger electron concentrations have the lower thermal conductivities because they have the greater densities of point defects to scatter phonons. Above 80 K, the larger electron-concentration samples have the higher thermal conductivities because they have the greater electronic heat transport. Thus, the total-thermal-conductivity curves for two samples with different electron concentrations intersect near 80 K.

In order to analyze the lattice thermal conductivity at all temperatures, it was necessary to determine what fraction of the total heat was transported by electrons. As a first step, the electronic thermal conductivity was calculated by using the values determined by AKS for  $L/L_0$  (see Fig. 5) in the modified Wiedemann-Franz law,

$$\kappa_E = (L/L_0) L_0 \sigma T, \quad (23)$$

where  $\kappa_E$  is the electronic thermal conductivity,  $L_0 = 2.44 \times 10^{-8} \text{ W } \Omega \text{ K}^{-2}$ ,  $\sigma$  is the electrical conduc-

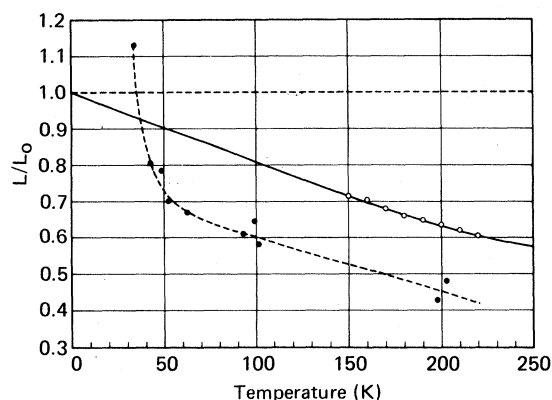


FIG. 5. Effective Lorenz number  $L/L_0$  as function of temperature for HgSe as determined by Aliev, Korenblit, and Shalyt (Ref. 13) (●) and by this work (○).

tivity, and  $T$  is the absolute temperature. The calculated electronic thermal conductivity was subtracted from the total thermal conductivity to obtain the lattice contribution only. However, when the values for  $L/L_0$  given by AKS were used, the resultant lattice thermal-conductivity curves for different samples still intersected. This implied that the calculated electronic thermal conductivity was too small, i. e., that the  $L/L_0$  values determined by AKS were too small. The reasons for the discrepancy when the  $L/L_0$  values of AKS were used may be deduced from the description of their experimental procedure. They measured the change in total thermal conductivity of a sample as a magnetic field was applied, and they assumed that all of the change resulted from a decrease in the electronic thermal conductivity. They maintained a constant influx of heat into the sample, and the sample mean temperature increased by 1–2 K when the magnetic field was fully applied. Above 100 K, a change in sample temperature of 1–2 K relative to the temperature of its enclosure results in a significant increase in heat radiated from the sample. Thus, as they applied a magnetic field to a sample, AKS were measuring not only a real change in thermal conductivity because of the decrease in the electronic part, but additionally an *apparent* change because of increased radiation loss from the sample. A 2-K increase of the sample mean temperature could easily have resulted in a radiation-loss error of magnitude comparable with the change in the electronic thermal conductivity.

It was necessary for us to independently determine the electronic thermal conductivity of each sample. This was done by an iterative procedure as follows.

(i) The total thermal conductivity at a given temperature  $T_i$  for a number of samples was

plotted against electrical conductivity. The points plotted were least-squares fitted by a straight line, the intercept of which at  $\sigma = 0$  was assumed to give the lattice thermal conductivity  $\kappa_0(T_i)$  of an ideal sample free of ionized impurities.

(ii) Approximate values for the Rayleigh scattering parameter  $A$  for the different samples were obtained by least-squares fitting the Callaway expression, Eq. (2), to the total-thermal-conductivity data for temperatures lower than 100 K, where the electronic contribution is small. The values for  $A$  so obtained were plotted against the electron concentration at 4.2 K and least-squares fitted by a straight line. The intercept of the line at  $n = 0$  gave a value  $A_0$  which was assumed to be the Rayleigh scattering parameter for an ideal sample free of ionized impurities.

(iii) The Callaway expression with  $A_0$  as the Rayleigh scattering parameter was fitted to the  $\kappa_0(T_i)$  values to obtain values for the other parameters. The parameters so obtained together with the approximate values of  $A$  for each sample then were used to calculate the lattice thermal conductivity of each sample at the temperatures  $T_i$ . By subtraction, the electronic thermal conductivity was obtained for each sample at each temperature  $T_i$ .

(iv) The electronic thermal conductivity was plotted against electrical conductivity for each temperature, and from the slope of the least-squares straight line passing through the origin the effective Lorenz number was calculated. This was done for temperatures from 150 to 220 K. Below 150 K, the electronic thermal conductivity was too small to be determined accurately, and above 220 K the possible errors caused by radiation loss were excessive. The Lorenz number for temperatures outside the range 150–220 K were obtained by extrapolation. The Lorenz-number curve as a function of temperature was extrapolated linearly from 150 to 0 K, with  $L/L_0$  assumed to be unity at 0 K, and extrapolated to higher temperatures by assuming constant curvature above 220 K. From the effective Lorenz-number curve so constructed, the electronic thermal conductivity as a function of temperature from 0 to 300 K was calculated for each sample and subtracted from the measured total thermal conductivity to obtain the lattice contribution.

(v) The lattice thermal-conductivity data for the different samples were again fitted by the Callaway expression, but this time over the complete temperature range for which data were obtained. The fits gave slightly revised values for the various scattering parameters. The revised values for  $A$  were plotted again as in step (ii) to obtain a revised value for  $A_0$ , and the succeeding steps were repeated. The cycle was repeated until no

changes were produced in the effective Lorenz numbers. This procedure necessarily yielded values for the effective Lorenz number of HgSe between 150 and 220 K which are consistent with our thermal-conductivity data. It has been assumed that the effective Lorenz number does not depend upon electrical conductivity and that the Rayleigh scattering parameter is a constant plus a term which increases linearly with electron concentration. Our results support these assumptions, at least for samples with  $n \leq 3.0 \times 10^{18} \text{ cm}^{-3}$ . The final curve obtained for  $L/L_0$  is shown in Fig. 5, and the plots of  $\kappa_E$  as a function of  $\sigma$  for eight different temperatures are shown in Fig. 6. Because of the scatter in the data and the difficulty of accurately calculating errors from radiation loss, it is difficult to establish the probable error of our  $L/L_0$  values. They cannot vary as much as  $\pm 10\%$ , however, and be consistent with the total-thermal-conductivity data unless our estimates of radiation-loss errors are incorrect by an order of magnitude.

Figure 7 shows the measured thermal conductivity, calculated radiation-loss error, electronic thermal conductivity, and resultant lattice thermal conductivity between 100 and 280 K for HgSe 3-2, a sample with a rather large concentration ( $3 \times 10^{18} \text{ cm}^{-3}$ ) of conduction electrons. The radiation-loss error and electronic contribution both are approximately the same as the lattice thermal conductivity at 280 K, and an error in determining the

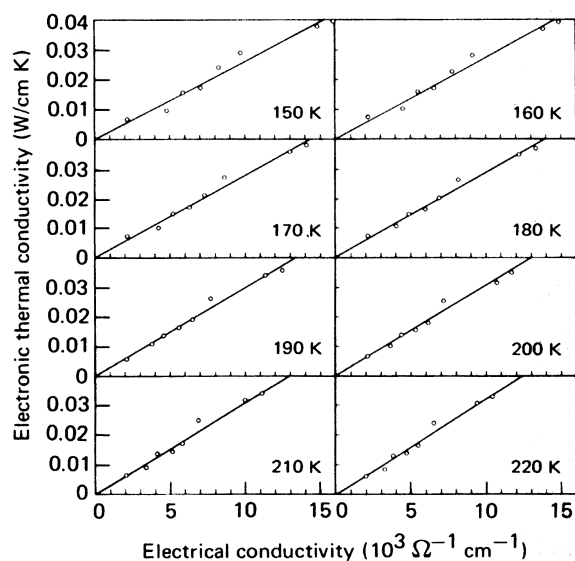


FIG. 6. Electronic thermal conductivity as function of electrical conductivity of HgSe at eight different temperatures. Data shown were deduced from measured total thermal conductivity. Slopes of least-squares straight-line fits were used to calculate effective Lorenz numbers shown in Fig. 5.

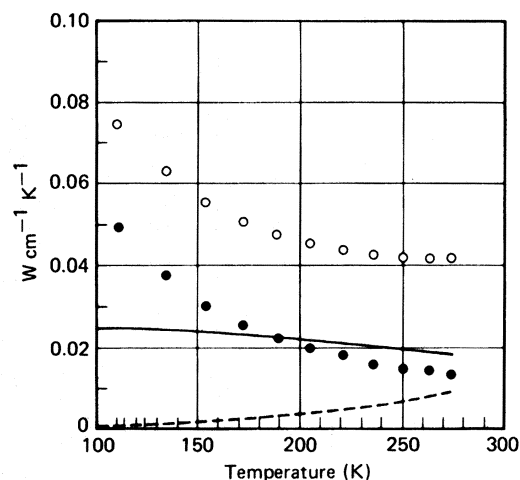


FIG. 7. Example of relative magnitudes of different contributions to measured thermal conductivity in the case of HgSe 3-2 with  $3.0 \times 10^{18} \text{ electrons/cm}^3$ . Shown are the measured thermal conductivity (O), the calculated subtractive radiation-loss correction (dashed line), the calculated electronic thermal conductivity (solid line), and the lattice thermal conductivity (●).

radiation loss or  $\kappa_E$  would cause a comparable relative error in the lattice thermal conductivity. The situation improves rapidly with decreasing temperatures because  $\kappa_E$  steadily becomes a smaller fraction of the total thermal conductivity and the radiation-loss error decreases and is negligible at 100 K.

#### V. THERMAL-CONDUCTIVITY CURVE FITTING

The lattice thermal-conductivity data for HgSe were fitted by adjusting the parameters  $B_1'$ ,  $B_2$ ,  $a$ ,  $F$ ,  $D$ ,  $A$ ,  $\omega_s$ ,  $\omega_a$ , and  $N$ .<sup>35</sup> The various scattering mechanisms assumed and the parameters associated with each are summarized in Table III. The sample cross-sectional dimensions are given in Table I, and the values calculated for  $m^*/m_e$  and  $\Theta_k$  are given in Table II. The average speed of sound in HgSe was calculated from the values at 4 K given by Lehoczky, Nelson, and Whitsett<sup>36</sup> for the longitudinal velocity  $v_l = 2.896 \times 10^5 \text{ cm/sec}$  and the transverse velocity  $v_t = 1.677 \times 10^5 \text{ cm/sec}$  in the  $\langle 100 \rangle$  direction. The average value used was

$$v = \frac{1}{3} \left( \frac{1}{v_l} + \frac{2}{v_t} \right)^{-1} = 1.95 \times 10^5 \text{ cm/sec} . \quad (24)$$

The value given by Lehoczky, Nelson, and Whitsett for the Debye temperature,  $\Theta = 151 \text{ K}$ , also was used. The value used for the density  $\rho$  was  $8.237 \text{ g/cm}^3$ , which was calculated from the weight change of HgSe single crystals when immersed in water. The Grüneisen constant  $\gamma$  was assumed to be 2.0.

TABLE III. Inverse relaxation times for various phonon scattering mechanisms used to curve-fit thermal-conductivity data. In these expressions,  $\Theta$  is the Debye temperature,  $v$  is the speed of sound,  $\alpha$  is the crystal cross-sectional area, and  $\Theta_k$  is the electron-phonon cutoff temperature. The variable parameters are  $B_1'$ ,  $B_2$ ,  $a$ ,  $\omega_s$ ,  $\omega_\alpha$ ,  $F$ ,  $A$ ,  $D$ , and  $N$ .

Umklapp processes	$\tau_U^{-1} = B_1' T \omega^2 e^{-\Theta/aT}$
Normal processes	$\tau_N^{-1} = B_2 T^3 \omega^2$
Boundary scattering	$\tau_B^{-1} = v/[F(1.12 \alpha^{1/2})]$
Rayleigh scattering	$\tau_A^{-1} = A \omega^4$
Electron-phonon scattering	$\tau_k^{-1} = D(m^*/m_e)^2 \omega \quad (\omega \leq K\Theta_k/\hbar),$ $= 0 \quad (\omega > K\Theta_k/\hbar)$
	$\tau_R^{-1} = \frac{9}{16} \frac{\pi^2}{\rho} \frac{\hbar \gamma^2}{v^2} \frac{\omega_s}{\omega_\alpha} N g(\omega) f(\omega, T) h(\omega),$
	$g(\omega) = \left(1 + \frac{4\omega_s}{\omega_\alpha}\right) \ln \left[ \left(\frac{\omega_\alpha}{\omega_s}\right) \left(\frac{\omega}{\omega_s}\right) \left(1 - \frac{\omega}{\omega_s}\right) + 1 \right] - \frac{4\omega}{\omega_s} \left(1 - \frac{\omega}{\omega_s}\right),$
Resonance scattering	$f(\omega, T) = \frac{(\omega_s - \omega)^2 e^{\hbar(\omega_s - \omega)/KT} (e^{\hbar\omega/KT} - 1)}{(e^{\hbar\omega_s/KT} - 1)(e^{\hbar(\omega_s - \omega)/KT} - 1)}$
	$h(\omega) = \begin{cases} \theta(\omega - \omega_s), & \omega_s \leq \omega_D \\ \theta(\omega_s - \omega_D - \omega)\theta(\omega - \omega_D), & \omega_s > \omega_D \end{cases}$
	$\theta(y) = \begin{cases} 1, & y \leq 0 \\ 0, & y > 0 \end{cases}$

The logarithm of the thermal conductivity given by Eq. (2) was fit to the logarithms of the measured values by the method of Marquardt<sup>37</sup> for the least-squares estimation of nonlinear parameters. If  $\kappa_i$  is the thermal conductivity measured for a sample at a temperature  $T_i$ , and if  $\kappa(T_i)$  is the value calculated at  $T_i$  from Eq. (2), then the curve fitting was done by finding the set of relaxation-time parameters which minimized

$$\Phi = \sum_{i=1}^r [\log_{10} \kappa_i - \log_{10} \kappa(T_i)]^2,$$

where  $r$  is the number of data points. The standard error for the fit to a set of data is  $S_0 = [\Phi_{\min}/(r-u)]^{1/2}$ , where  $u$  is the number of adjustable parameters. Confidence limits for the values of the parameters which minimized  $\Phi$  were calculated by finding the lower and upper limits of the range of values of each parameter which gave a  $\Phi$  such that  $(\Phi - \Phi_{\min})/uS_0^2 \leq \mathcal{F}$ . The variance ratio  $\mathcal{F}$  in each case was so chosen that the probability was 0.990 that the true value of a parameter lay between the lower and upper confidence limits.<sup>38</sup>

Because there was no reason to believe that the umklapp and normal scattering should vary from sample to sample, the data for HgSe 3-2, 3-3, 3-4, 3-5, 4-1, and 5-1 were fit simultaneously with the restriction that  $B_1'$ ,  $B_2$ ,  $a$ , and  $D$  be the same for all of the samples. The results of this "group" fit to a total of 267 data points with 22 adjustable parameters are compiled in Table IV. The range for each parameter within which the probability is

0.990 that the true value of the parameter is included is indicated by the plus and minus increments in Table IV. The calculation of the confidence limits assumes, of course, that the theoretical model used to fit the data is perfect. (Also included in Table IV are parameters for HgSe 3-6 and 4-2 which were not included in the group fitting; the data below 4 K for these samples were anomalous, possibly because of diffusion of indium solder into the crystals.) The lattice thermal-conductivity data that were fitted are plotted in Figs. 8-10, and the least-squares-fit curves calculated from Eq. (2) and the parameters in Table IV are shown. Also shown for each sample in Figs. 8-10 is the calculated electronic thermal conductivity, which was subtracted from the data in Figs. 2-4 to obtain the lattice thermal conductivity.

The values for the parameters  $B_1'$ ,  $B_2$ , and  $a$  required to fit the data have the magnitudes usually found for other materials. The theoretical basis for none of these parameters is good, and because of the oversimplification of our model for thermal conductivity there is no reason to believe that the precise values of these parameters have significance. The parameter  $B_1'$  in the expression for the umklapp relaxation time, Eq. (7), is  $2.19 \times 10^{-17} \text{ sec K}^{-1}$ . The formula of Slack and Galginaitis,<sup>23</sup> Eq. (8), gives in the case of HgSe,  $B_1' = 3.21 \times 10^{-18} \text{ sec K}^{-1}$ , a value about one-seventh of that determined by curve fitting. The parameter  $a$  in the exponential factor for umklapp scattering

TABLE IV. Phonon scattering parameters determined by curve fitting the thermal-conductivity data of all HgSe samples simultaneously. In addition to  $B_1'$ ,  $B_2$ , and  $a$ , the electron-phonon scattering parameter  $D$  was required to be the same for all samples. The least-squares fit was obtained with  $B_1' = (2.19 \pm 0.14) \times 10^{-17} \text{ sec K}^{-1}$ ,  $B_2 = (3.01 \pm 0.77) \times 10^{-22} \text{ sec K}^{-3}$ ,  $a = 1.23 \pm 0.06$ ,  $\omega_s = 4.32 \times 10^{12} \text{ sec}^{-1}$ , and  $D = (8.50 \pm 1.63) \times 10^{-5}$ . Standard deviation for the group fit was  $S_0 = 0.02586$ . Probability is 99.0% that true value of a parameter is within the given plus and minus increments.

HgSe sample No.	$F$	$10^{44} A$ (sec <sup>3</sup> )	$10^{-19} N$ (cm <sup>-3</sup> )	Standard error
3-2	1.8 (+1.2, -0.4)	327 (+44, -39)	436 (+111, -90)	0.03230
3-3	6.0 (+8.2, -1.9)	108 (+17, -15)	193 (+49, -66)	0.03318
3-4	4.4 (+6.5, -1.2)	114 (+20, -16)	222 (+61, -50)	0.01451
3-5	0.85 (+0.48, -0.26)	362 (+50, -43)	378 (+105, -82)	0.02513
3-6 <sup>a</sup>	0.31	151	228	0.01641
4-1	136 <sup>b</sup>	94 (+15, -13)	237 (+55, -46)	0.02050
4-2 <sup>a</sup>	0.22	331	436	0.01766
5-1	788 <sup>b</sup>	232 (+33, -20)	376 (+90, -74)	0.01961

<sup>a</sup>HgSe samples 3-6 and 4-2 were not included in group fitting.

<sup>b</sup>Nonlinear confidence limits could not be found.

should be of the order unity, and the value of 1.23 found for  $a$  is reasonable. The value of  $B_1'$  for HgSe is larger than that reported<sup>21</sup> for the related compound HgTe ( $9.30 \times 10^{-18} \text{ sec K}^{-1}$ ), but the values found for  $B_2$  ( $3.01 \times 10^{-22} \text{ sec K}^{-3}$ ) and for  $a$  (1.23) are essentially the same as those ( $B_2 = 3.00 \times 10^{-22} \text{ sec K}^{-3}$  and  $a = 1.30$ ) for HgTe.

The boundary scattering parameter  $F$  can range from unity for completely diffuse reflection of phonons at the crystal boundaries to infinity for completely specular reflection, but for most materials it is found experimentally to be of the order of uni-

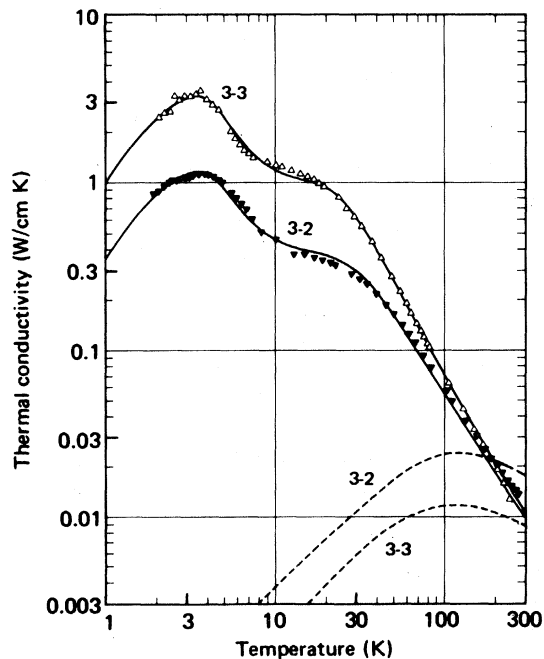


FIG. 8. Lattice thermal conductivity of HgSe 3-2 ( $\blacktriangledown$ ) and HgSe 3-3 ( $\Delta$ ). HgSe 3-2 was as-grown and had  $3.0 \times 10^{18} \text{ electrons/cm}^3$ ; HgSe 3-3 was vacuum annealed and had  $5.7 \times 10^{17} \text{ electrons/cm}^3$  at 4.2 K. The solid lines were calculated by using the parameters of Table IV in the Callaway formulation. The dashed lines are the calculated electronic thermal conductivities.

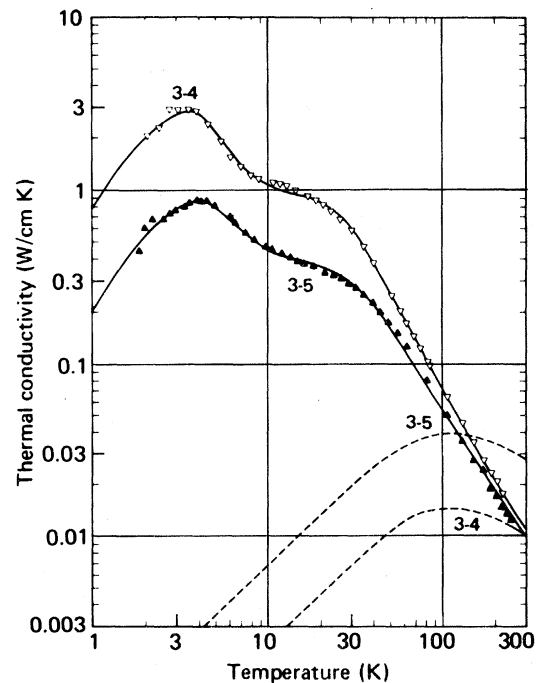


FIG. 9. Lattice thermal conductivity as function of temperature for HgSe 3-4 ( $\nabla$ ) and HgSe 3-5 ( $\blacktriangle$ ). HgSe 3-4 was Se-vapor annealed and had  $8.0 \times 10^{17} \text{ electrons/cm}^3$  at 4.2 K; HgSe 3-5 was Hg-vapor annealed and had  $6.7 \times 10^{18} \text{ electrons/cm}^3$ . The solid lines were calculated by using the parameters of Table IV in the Callaway formulation. The dashed lines are the calculated electronic thermal conductivities.

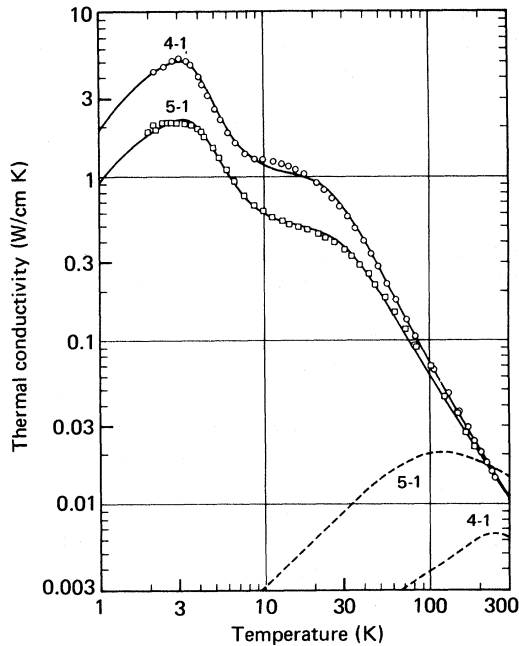


FIG. 10. Lattice thermal conductivity as function of temperature for HgSe 4-1 (○) and HgSe 5-1 (□). HgSe 4-1 was vacuum annealed and had  $2.1 \times 10^{17}$  electrons/cm<sup>3</sup> at 4.2 K; HgSe 5-1 was as-grown and had  $2.2 \times 10^{18}$  electrons/cm<sup>3</sup>. The solid lines were calculated by using the parameters of Table IV in the Callaway formulation. The dashed lines are the calculated electronic thermal conductivities.

ty. In Table IV the large values listed for  $F$  resulted from the curve-fitting program virtually eliminating the boundary scattering term from the mean free time to achieve a minimum sum of squares. If the data had extended to lower temperatures, the electron-phonon scattering term could have been established with much greater confidence, and the values then obtained for  $F$  would have been more significant. (The data could be fitted equally well by omitting the electron-phonon scattering term and allowing  $F$  to vary freely to limit the calculated low-temperature thermal conductivity. However, this resulted in values for  $F$  considerably smaller than unity for the samples with electron concentrations greater than  $1 \times 10^{18}$  cm<sup>-3</sup>, and this is not reasonable physically.)

The parameter  $D$ , given by Eq. (16), was determined to be  $8.50 \times 10^{-5}$ , and this implies a value for the deformation potential of 0.68 eV. As was mentioned previously, the  $p^{3/2}$ -like symmetry of the conduction-band wave functions allows electronic scattering of both longitudinal and transverse phonons. Moreover, the deformation potential associated with longitudinal-phonon scattering by the  $s$ -like electrons of a normal semiconductor is replaced by five irreducible matrix elements,<sup>39</sup> and

complicated angular dependences appear in the differential scattering cross section. Thus, the value of 0.68 eV for the deformation potential has significance only as a lumped parameter required to fit the data.

The Rayleigh scattering parameter, although strongly statistically correlated with the resonance scattering coefficient  $N$ , was determined with relatively high confidence. In Fig. 11 both  $A$  and  $N$  are plotted as functions of the low-temperature electron concentration  $n$ . If the conduction electrons are contributed by excess interstitial mercury atoms, then for each electron there should be one point defect and  $A$  should be a linear function of the electron concentration. For electron concentrations up to  $3 \times 10^{18}$  cm<sup>-3</sup>, the values determined for  $A$  do vary approximately linearly with  $n$ , and the straight-line least-squares fit to the data is represented by

$$A = 5.7 \times 10^{-43} \text{ sec}^3 + (8.4 \times 10^{-61} \text{ sec}^3 \text{ cm}^3)n. \quad (25)$$

However, for  $n \geq 3 \times 10^{18}$  cm<sup>-3</sup>, the Rayleigh scattering parameter no longer varies linearly with the electron concentration and had, for three samples, an average value of  $3.4 \times 10^{-42}$  sec<sup>3</sup>.

The concentration-dependent term in Eq. (25) for  $n < 3.0 \times 10^{18}$  cm<sup>-3</sup> is given by Eq. (13) if  $n$  is substituted for  $N_i$  and if  $S_i = 1.43$ . The constant term in Eq. (25) is larger than  $A_{\text{isot}}$  [Eq. (11)] by more than an order of magnitude, and such a discrepancy implies that other, neutral, Rayleigh scattering centers were present. A simple hypothesis is that each sample had a concentration of neutral defects of  $1.3 \times 10^{18}$  cm<sup>-3</sup> with unity scattering factors. Then Eq. (13) yields a neutral defect contribution to  $A$  of  $5.3 \times 10^{-43}$  sec<sup>3</sup>, which

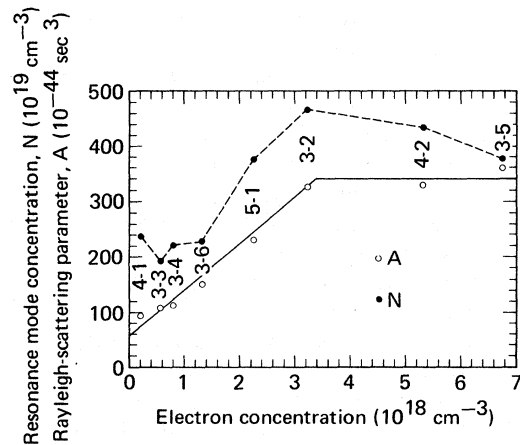


FIG. 11. Rayleigh phonon scattering parameter  $A$  (○) and resonance mode density  $N$  (●) as functions of conduction-electron concentration. Parameters  $A$  and  $N$  are those given in Table IV and were determined by curve fitting thermal-conductivity data.

TABLE V. Phonon scattering parameters determined by curve fitting the thermal-conductivity data of all HgSe samples simultaneously. (HgSe samples 3-6 and 4-2 were not included in group fitting.) In addition to  $B_1'$ ,  $B_2$ ,  $a$ , and  $D$ , the concentration  $N$  of resonantly scattering modes was required to be the same for all samples. The least-squares fit was obtained with  $B_1' = 2.17 \times 10^{-17} \text{ sec K}^{-1}$ ,  $B_2 = 2.43 \times 10^{-22} \text{ sec K}^{-3}$ ,  $\alpha = 1.33$ ,  $\omega_s = 4.44 \times 10^{12} \text{ sec}^{-1}$ ,  $D = 8.45 \times 10^{-5}$ , and  $N = 349 \times 10^{19} \text{ cm}^{-3}$ . Standard error for the group fit was  $S_0 = 0.03085$ .

HgSe sample No.	$F$	$10^{44} A$ (sec <sup>3</sup> )
3-2	2.0	368
3-3	3.0	69
3-4	2.6	82
3-5	0.84	374
4-1	20	69
5-1	161	240

added to the calculated value of  $A_{\text{tot}}$  gives the constant term in Eq. (25). This concentration of neutral defects is about the same as that postulated<sup>11</sup> to explain the anomalous electron mobility in  $\alpha$ -Sn. The low-electron-concentration samples of HgSe used in this study have mobilities which are comparable with those of  $\alpha$ -Sn samples, i. e., considerably lower than the theoretically expected values. To test the hypothesis that the additional electron scattering is from neutral defects, the Rayleigh scattering parameter  $A$  should be examined for low-electron-concentration samples whose mobilities approach more closely the theoretical values.

The value obtained for  $\omega_\alpha$ ,  $3.3 \times 10^{12} \text{ sec}^{-1}$ , implies a radius of  $\alpha_c^{-1} \approx 6 \times 10^{-8} \text{ cm}$  for the resonant centers. However, the curve fitting was quite insensitive to changes in  $\omega_\alpha$ , and  $\omega_\alpha$  could be increased or decreased an order of magnitude without significantly increasing the standard error of the fit. The value of  $\omega_s$ ,  $4.32 \times 10^{12} \text{ sec}^{-1}$ , implies that the resonance lies within the acoustic-phonon band; that is, the resonance is a quasilocalized mode. The values for  $N$ , the density of resonance modes, had high statistical correlation with the Rayleigh scattering parameter values. The best fit gave values for  $N$  between  $1.9 \times 10^{21}$  and  $4.4 \times 10^{21} \text{ cm}^{-3}$ . Such large values for  $N$  certainly are not reasonable, even if one assumes that a resonant complex extends to second nearest neighbors of the responsible lattice defect. Errors of this sort are typical of calculations for third-order processes in crystals with unit cells whose non-equivalent atoms have greatly differing masses.<sup>40</sup> It is not known whether they are associated with dispersion,<sup>41,42</sup> that is, violation of the Debye approximation, or with breakdown of the "Grüneisen

approximation" [Eq. (38) of Ref. 32]. Additional work, done in an attempt to identify the resonant scatterers, will be described in Sec. VI.

## VI. RESONANCE SCATTERING

The resonance scattering mode density  $N$ , plotted as a function of electron concentration in Fig. 11, has behavior resembling that of the Rayleigh scattering parameter  $A$ . However, the data for all the samples collectively also could be fitted rather well (with a standard error of 0.03085) by assuming that  $N$  is constant for all samples. The results of such a fit are compiled in Table V. The constant value obtained for  $N$  was  $3.49 \times 10^{21} \text{ cm}^{-3}$ . The values obtained for  $A$  are different, but the dependence of  $A$  upon  $n$  is unchanged qualitatively. Thus, data for many more samples would be required to definitely establish if  $N$  varies randomly around a mean value from sample to sample or is correlated with  $n$  and  $A$ .

If the resonance scattering is due to a chemical impurity, the most likely candidates are substitutional oxygen, sulfur, and tellurium. It is difficult to quantitatively analyze for these elements in HgSe, but chemical analyses indicated that Te, if present at all, was less than 10 ppm by weight and that S was present in concentrations possibly as large as 20–30 ppm by weight in all samples. Although the resonance frequency lies within the acoustic band, the lighter elements, oxygen and sulfur, cannot be eliminated from consideration. Takeno<sup>43</sup> has pointed out that for a light impurity, even without softening of force constants, there is a solution of the defect matrix lying within the band in addition to the solution for the true localized mode lying outside the band.

To determine if substitutional oxygen was important in the resonance scattering of phonons, a sample of HgSe was prepared which should have had a significantly lower oxygen concentration than that of the other samples. A specially constructed quartz distillation apparatus was used to triply distill the Hg and Se starting material; the distillations were performed and the elements distilled into the crystal preparation capsule without exposing any of the material to air. Before each distillation the materials were heated and outgassed in a vacuum of pressure less than  $1 \times 10^{-6}$  Torr. The outgassing temperature for Se was 250 °C, a temperature high enough to decompose  $\text{SeO}_3$  to Se. The thermal conductivity (shown in Fig. 12) of crystal HgSe 6-1 grown from the triply distilled and degassed elements was identical with the thermal conductivity of other HgSe crystals that had the same electron concentration. Although the oxygen content of HgSe 6-1 relative to that of the other crystals was not determined, it should have been smaller, and the magnitude of the resonance

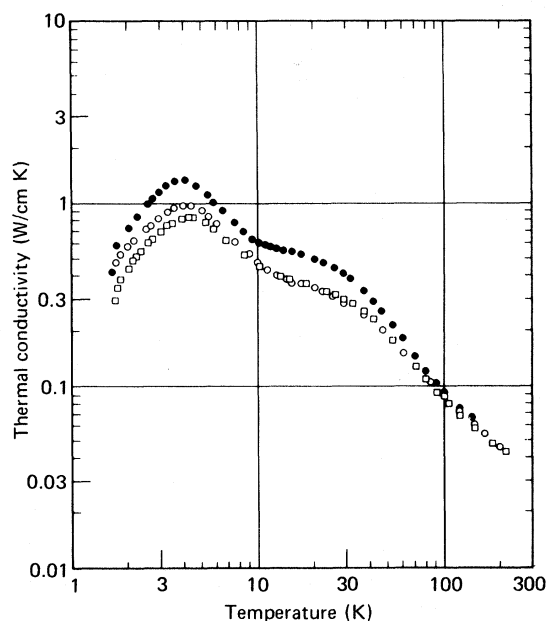


FIG. 12. Total thermal conductivity of HgSe 6-1 ( $\circ$ ), grown from vacuum-distilled Hg and Se; HgSe 7-1 ( $\square$ ), grown with excess Hg; and vapor-grown HgSe ( $\bullet$ ).

should have been slightly smaller if interstitial oxygen were important; however, the resonance was unchanged.

Another crystal, HgSe 7-1, was grown from a melt which contained a 6-wt% excess of Hg to determine if an increased Hg vapor pressure at the time of crystallization had an effect on the resonance scattering. The thermal conductivity of HgSe 7-1, also shown in Fig. 12, was identical with that of other crystals which had comparable electron concentrations. Finally, the thermal conductivity (shown in Fig. 12) of a HgSe crystal grown from vapor on a substrate at 500 °C was measured and was identical with that of crystals grown from a melt.

To determine if substitutional sulfur plays a role in the resonance effect, two HgSe crystals were prepared with added sulfur impurity. The first of these, HgSe S1, contained  $5.0 \times 10^{19}$  atoms/cm<sup>3</sup> of S substituted for Se; the second, HgSe S2, contained  $5.0 \times 10^{20}$  atoms/cm<sup>3</sup> of S substituted for Se. These sulfur concentrations are, respectively, 0.14 and 1.4 at. % compared with approximately 0.011 at. % ( $\sim 4 \times 10^{18}$  atoms/cm<sup>3</sup>) possibly present in the undoped HgSe. The sulfur-doped crystals were subjected to annealing in vacuum and in Hg vapor, and their lattice thermal conductivities were determined by the methods used for the undoped samples. The lattice thermal conductivities of HgSe S1-1 (vacuum annealed) and HgSe S1-2 (Hg-vapor annealed) are shown in Fig. 13, and of HgSe S2-1 (vacuum annealed) and HgSe S2-2 (Hg-

vapor annealed) in Fig. 14. The addition of S to HgSe lowered the higher-temperature lattice thermal conductivity, and the data for the sulfur-doped crystals could not be fitted satisfactorily by using the umklapp and normal scattering parameters that fit the data for undoped crystals. The samples S1-1 and S1-2 were fitted simultaneously with only  $F$ ,  $A$ , and  $N$  allowed to vary between samples, and the data for HgSe S2-1 and S2-2 similarly were fitted simultaneously. The parameters which gave the least-squares fits are compiled in Table VI. The Rayleigh scattering parameter increased with increased sulfur doping as is to be expected. Additionally, both the resonant frequency  $\omega_s$  and the resonant mode density  $N$  increased with sulfur doping.

The addition of sulfur clearly affects the resonance scattering of phonons in HgSe, but it cannot be concluded from the results presented here that substitutional S atoms are the resonance centers. The change in the lattice dynamics of HgSe upon the addition of sulfur, as evidenced by the changes in the umklapp and normal scattering parameters, would considerably affect the nature of the resonance scattering whatever the identity of the resonance centers. Furthermore, in the sulfur-doped HgSe crystals, the increase in  $N$  with an increase

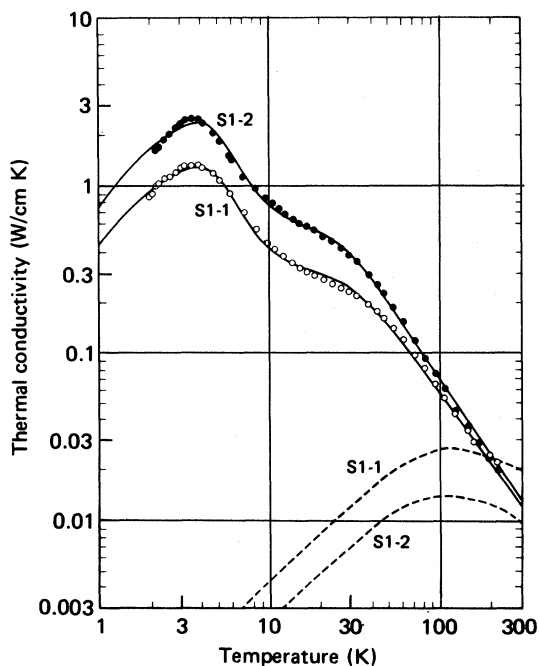


FIG. 13. Lattice thermal conductivity as function of temperature for HgSe doped with  $5 \times 10^{19}$  S atoms/cm<sup>3</sup>. HgSe S1-1 ( $\circ$ ) was as-grown and had  $4.2 \times 10^{18}$  electrons/cm<sup>3</sup>; HgSe S1-2 ( $\bullet$ ) was vacuum annealed and had  $8.5 \times 10^{17}$  electrons/cm<sup>3</sup> at 4.2 K. Solid lines were calculated by Callaway formulation. The dashed lines are the calculated electronic thermal conductivities.

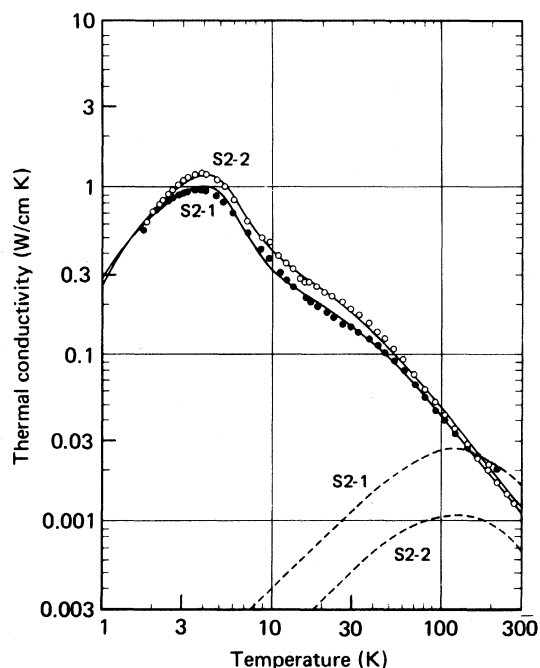


FIG. 14. Lattice thermal conductivity as function of temperature for HgSe doped with  $5 \times 10^{20}$  S atoms/cm<sup>3</sup>. HgSe S2-1 (●) was as-grown and had  $4.0 \times 10^{18}$  electrons/cm<sup>3</sup>; HgSe S2-2 (○) was vacuum annealed and had  $4.9 \times 10^{17}$  electrons/cm<sup>3</sup> at 4.2 K. Solid lines were calculated by using the parameters of Table VI in the Callaway formulation. The dashed lines are the calculated electronic thermal conductivities.

in electron concentration is about the same as for undoped crystals.

The only other low-temperature thermal-conductivity data for HgSe in the literature is that of Aliev, Korenblit, and Shalyt.<sup>13</sup> Their data for a HgSe single crystal with  $5.0 \times 10^{17}$  electrons/cm<sup>3</sup> are reproduced in Fig. 15, and for comparison our data for HgSe 3-3 with  $n = 5.7 \times 10^{17}$  electrons/cm<sup>3</sup> are shown also. Above 8 K, the two sets of data are the same to within experimental error. However, their data do not exhibit any trace of a resonance dip and fall off much too rapidly with decreasing temperature to be explained by boundary scattering and elec-

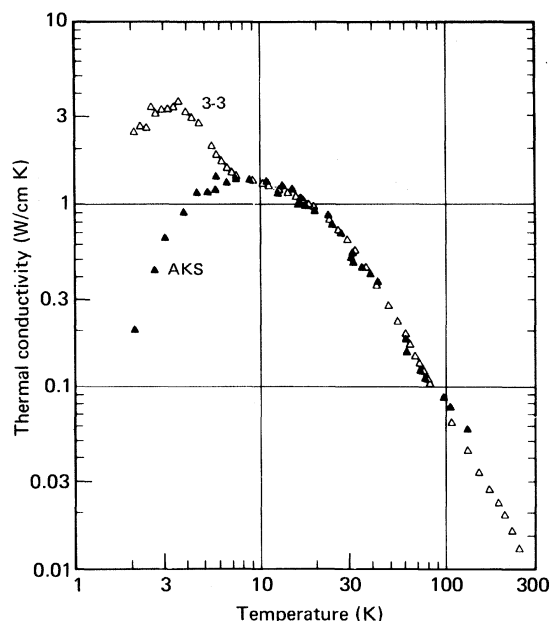


FIG. 15. Comparison of lattice thermal-conductivity results of Aliev, Korenblit, and Shalyt (Ref. 13) for HgSe with  $5 \times 10^{17}$  electrons/cm<sup>3</sup> (▲) and for HgSe 3-3 with  $5.7 \times 10^{17}$  electrons/cm<sup>3</sup> at 4.2 K (Δ).

tron-phonon scattering. It cannot be argued that the sample measured by Aliev, Korenblit, and Shalyt was more pure than ours and therefore had a negligible number of resonance centers, because if that were true, the thermal conductivity of their sample should have had a maximum value larger than that measured for our samples. As Fig. 15 shows, we measured a maximum nearly four times larger than they did. To explain their results for temperatures below 8 K, some additional phonon scattering mechanism, not present in our crystals, must be assumed.

## VII. DISCUSSION

Although the general mechanisms of phonon scattering in HgSe have been established, the identity of and relations between the scattering centers are far from clear. Of particular importance are the

TABLE VI. Phonon scattering parameters determined by curve fitting the thermal-conductivity data of sulfur-doped HgSe single crystals. Samples S1-1 and S1-2 were fit simultaneously with only  $F$ ,  $A$ , and  $N$  permitted to vary between samples. Samples S2-1 and S2-2 similarly were fit simultaneously. The value used for  $D$  was that given in Table V.

HgSe sample No.	S atoms added per cm <sup>3</sup>	$10^{17} B_1'$ (sec K <sup>-1</sup> )	$10^{22} B_2$ (sec K <sup>-3</sup> )	$a$	$10^{-12} \omega_s$ (sec <sup>-1</sup> )	$F$	$10^{44} A$ (sec <sup>3</sup> )	$10^{-19} N$ (cm <sup>-3</sup> )	Standard error
S1-1	$5 \times 10^{19}$	1.91	1.10	1.43	5.22	4.8	388	601	0.02284
S1-2							205	353	
S2-1	$5 \times 10^{20}$	1.19	5.18	3.04	5.50	1.6	418	959	0.02378
S2-2						0.93	293	790	

relation between  $N$  and  $A$  and the apparent leveling off of the number of Rayleigh scatterers above an electron concentration of  $3 \times 10^{18} \text{ cm}^{-3}$ .

The first and simplest explanation of the leveling off of  $A$  is that the theory of Rayleigh scattering becomes invalid for defect concentrations larger than  $3 \times 10^{18} \text{ cm}^{-3}$ . Such a sharp cutoff is unlikely, although in the temperature range for which Rayleigh scattering dominates, the wavelength of phonons conveying the maximum heat current per unit energy does approach the distance between scatterers at this concentration. If the theory is accepted as valid, then a number of other hypotheses can be formed.

First, assume that the ionized impurities and the resonant scatterers are one and the same species. Then, the leveling off of  $A$  may be explained as the appearance of a second ionization state with a Rayleigh scattering cross section not markedly different from that of the singly ionized state. The change of ionization state would certainly change the localized modes, and indeed one does see an apparent decrease in the resonance mode density of samples with more than  $3 \times 10^{18} \text{ electrons/cm}^3$ . However, two factors mitigate against this hypothesis: The change in  $N$  is not large enough to account for the added electrons, and the samples with  $n \geq 3 \times 10^{18} \text{ cm}^{-3}$  have electron mobilities closer to the theoretical values than those with  $n < 3 \times 10^{18} \text{ cm}^{-3}$ . Doubly charged centers would cause mobilities to be more divergent from the theoretical values.

Second, it might be assumed that the resonant scatterers are neutral and distinct from the ionized defects, and that the leveling off of  $A$  is again produced by the appearance of a second ionization of the ionized defects. The same objection concerning the mobility detracts from this hypothesis as well as the first.

Third, one can assume again that the resonant scatterers and ionized impurities are distinct species, but that the additional electrons above  $3 \times 10^{18} \text{ cm}^{-3}$  result from ionization of the neutral resonant scatterers. This would account for both the apparent leveling off of  $A$  and the decrease in  $N$ .

Whatever the cause of the nonlinear behavior of  $A$ , it may well be related to another characteristic of HgSe, namely, that samples which have either less than or more than about  $(2-3) \times 10^{18}$

electrons/cm<sup>3</sup> change with time at room temperature and tend towards having electron concentrations of about  $(2-3) \times 10^{18} \text{ cm}^{-3}$ . This has been our observation as well as that of others.<sup>44,45</sup>

Although the resonance mode density increases with sulfur concentration in the heavily doped samples, this does not indicate that the substitutional sulfur atoms are the source of the resonant scattering, since the increase in mode density is quite small in comparison with the increase in sulfur concentration. It is more likely that this effect, along with the change in  $\omega_s$ , is due to a change in the environment of the resonant scatterers.

In order to settle these questions concerning the identity of the scattering centers and the leveling off of  $A$ , a larger number of high-concentration samples would have to be examined. It would also be useful to have far-infrared reflectivity or Raman observations of the localized modes to aid in their identification. Grynberg, Le Toulec, and Balkanski<sup>46</sup> have recently observed a strongly temperature-dependent structure in the far-infrared reflectivity of HgTe which they interpret to be a localized mode produced by a very large defect density. This mode, however, is a gap mode. It may be significant that HgTe, which always grows  $p$  type, has a high-frequency gap mode while HgSe, which always grows  $n$  type, has a low-frequency mode within the acoustic branches.

Sherrington<sup>12</sup> has recently predicted that the acoustic modes of the zero-gap structures, because of the unusual singular properties of their dielectric functions, should have two regions of linear dispersion separated by a transition region around the Fermi momentum of the electron gas. It should be noted that at the lowest temperatures of this experiment, most of the heat current is carried by phonons with wave vectors smaller than the Fermi momentum. Thus, if a quantitative microscopic theory of heat conduction in these structures at low temperatures were available, a low-temperature thermal-conductivity experiment might provide a convenient method of detecting this anomalous phonon dispersion.

#### ACKNOWLEDGMENTS

We are grateful to Dr. D. P. Ames for his support of this research and for helpful discussions. We also thank Dr. S. L. Lehoczky who assisted with many of the measurements.

\*Research conducted under the McDonnell Douglas Independent Research and Development Program.

<sup>1</sup>Presently with McDonnell Aircraft Company, St. Louis, Mo. 63166.

<sup>2</sup>For reviews of the general properties of HgSe, see T. C. Harman, in *Physics and Chemistry of II-VI Compounds*, edited by M. Aven and J. S. Prener (North-Holland, Amsterdam,

1967), Chap. 15, p. 767; T. C. Harman, in *II-VI Semiconducting Compounds, 1967 International Conference*, edited by D. G. Thomas (Benjamin, New York, 1967), p. 982.

<sup>3</sup>S. Groves and W. Paul, *Phys. Rev. Lett.* **11**, 194 (1963).

<sup>4</sup>S. H. Groves, R. H. Brown, and C. R. Pidgeon, *Phys. Rev.* **161**, 779 (1967).

<sup>5</sup>J. G. Broerman, *Phys. Rev.* **183**, 754 (1969).

- <sup>5</sup>S. Bloom and T. K. Bergstresser, *Phys. Status Solidi* **42**, 191 (1970).
- <sup>6</sup>C. R. Whitsett, S. L. Lehoczky, and J. G. Broerman, *Bull. Am. Phys. Soc.* **15**, 315 (1970).
- <sup>7</sup>L. Liu and D. Brust, *Phys. Rev. Lett.* **20**, 651 (1968).
- <sup>8</sup>D. Sherrington and W. Kohn, *Phys. Rev. Lett.* **21**, 153 (1968).
- <sup>9</sup>J. G. Broerman, *Phys. Rev. Lett.* **25**, 1658 (1970); *Phys. Rev. B* **5**, 397 (1972).
- <sup>10</sup>J. G. Broerman, *Phys. Rev. B* **1**, 4658 (1970); *Phys. Rev. B* **2**, 1818 (1970).
- <sup>11</sup>J. G. Broerman, *J. Phys. Chem. Solids* **32**, 1263 (1971).
- <sup>12</sup>D. Sherrington, *J. Phys. C* **4**, 2771 (1972).
- <sup>13</sup>S. A. Aliev, L. L. Korenblit, and S. S. Shalyt, *Fiz. Tverd. Tela* **8**, 705 (1966) [*Sov. Phys.-Solid State* **8**, 565 (1966)].
- <sup>14</sup>A. V. Ioffe and A. F. Ioffe, *Fiz. Tverd. Tela* **2**, 781 (1960) [*Sov. Phys.-Solid State* **2**, 719 (1960)].
- <sup>15</sup>M. Rodot, H. Rodot, and R. Triboulet, *J. Appl. Phys.* **32**, 2254 (1961).
- <sup>16</sup>C. R. Whitsett, *J. Appl. Phys.* **32**, 2257 (1961).
- <sup>17</sup>T. C. Harman, *J. Phys. Chem. Solids* **25**, 931 (1964).
- <sup>18</sup>F. Kelemen, E. Cruceanu, and D. Niculescu, *Phys. Status Solidi* **11**, 865 (1965).
- <sup>19</sup>I. A. Smirnov and S. A. Aliev, *Fiz. Tverd. Tela* **10**, 2643 (1968) [*Sov. Phys.-Solid State* **10**, 2080 (1969)].
- <sup>20</sup>C. R. Whitsett and D. A. Nelson, *J. Cryst. Growth* **6**, 26 (1969).
- <sup>21</sup>C. R. Whitsett and D. A. Nelson, *Phys. Rev. B* **5**, 3125 (1972).
- <sup>22</sup>J. Callaway, *Phys. Rev.* **113**, 1046 (1959).
- <sup>23</sup>G. A. Slack and S. Galginitis, *Phys. Rev.* **133**, A253 (1964).
- <sup>24</sup>P. G. Klemens, *Proc. Phys. Soc. Lond. A* **68**, 1113 (1955).
- <sup>25</sup>H. E. Swanson, N. T. Gilfrich, and M. I. Cook, *Circ. U.S. Natl. Bur. Std.* **7**, 35 (1957).
- <sup>26</sup>H. B. G. Casimir, *Physica (Utr.)* **5**, 47 (1938); *Physica (Utr.)* **5**, 320 (1938); *Physica (Utr.)* **5**, 619 (1938).
- <sup>27</sup>R. Berman, F. E. Simon, and J. M. Ziman, *Proc. R. Soc. A* **220**, 171 (1953).
- <sup>28</sup>R. Berman, E. L. Foster, and J. M. Ziman, *Proc. R. Soc. A* **231**, 130 (1955).
- <sup>29</sup>See, for example, J. M. Ziman, *Electrons and Phonons* (Oxford U. P., London, 1963), p. 330.
- <sup>30</sup>E. O. Kane, *J. Phys. Chem. Solids* **1**, 249 (1957).
- <sup>31</sup>C. R. Whitsett, *Phys. Rev.* **138**, A829 (1965).
- <sup>32</sup>M. Wagner, *Phys. Rev.* **131**, 1443 (1963).
- <sup>33</sup>J. A. Krumhansl, in *Proceedings of the International Conference on Lattice Dynamics, Copenhagen, 1963*, edited by R. F. Wallis (Pergamon, Oxford, England, 1964), p. 523.
- <sup>34</sup>M. G. Holland, *Phys. Rev.* **132**, 2461 (1963).
- <sup>35</sup>In a preliminary report [D. A. Nelson, J. G. Broerman, E. C. Paxhia, and C. R. Whitsett, *Phys. Rev. Lett.* **22**, 884 (1969)], a similar analysis was presented for HgSe 3-2, 3-3, 3-4, and 3-5 (denoted, respectively, as runs 1-4). In this earlier paper, the data had not been corrected for radiation-loss errors, the electronic thermal conductivity was underestimated, and boundary scattering alone was assumed to dominate at low temperatures. The combination of these factors was responsible for the scattering parameter values then reported being different from the values given here.
- <sup>36</sup>A. Lehoczky, D. A. Nelson, and C. R. Whitsett, *Phys. Rev.* **188**, 1069 (1969).
- <sup>37</sup>D. W. Marquardt, *J. Soc. Ind. Appl. Math.* **11**, 431 (1963).
- <sup>38</sup>The probability for the confidence limits was based upon Snedecor's  $F$  (variance ratio) distribution tables in *Handbook of Mathematical Functions*, edited by M. Abramowitz and I. A. Stegun, *Natl. Bur. Std. (U. S.) Appl. Math. Ser. 55* (U. S. GPO, Washington, D. C., 1964), pp. 986-9.
- <sup>39</sup>W. Zawadski and W. Szymanska, *Phys. Status Solidi* **45**, 415 (1971).
- <sup>40</sup>P. G. Klemens, *Solid State Phys.* **7**, 1 (1958).
- <sup>41</sup>G. Leibfried, in *Handbuch der Physik*, edited by S. Flügge (Springer-Verlag, Berlin, 1955), Vol. 7, Pt. I, p. 104.
- <sup>42</sup>M. Blackman, *Philos. Mag.* **19**, 989 (1935).
- <sup>43</sup>S. Takeno, *Prog. Theor. Phys.* **29**, 191 (1963).
- <sup>44</sup>G. B. Wright, A. J. Strauss, and T. C. Harman, *Phys. Rev.* **125**, 1534 (1962).
- <sup>45</sup>R. R. Galazka, W. M. Becker, and D. G. Seiler, in *Physics of Semimetals and Narrow-Gap Semiconductors*, edited by D. L. Carter and R. T. Bate (Pergamon, New York, 1971), p. 481.
- <sup>46</sup>M. Grynberg, R. Le Toullec, and M. Balkanski, *Phys. Rev. B* (to be published).

## Ultrasonic Attenuation in Pure and Doped $n$ -Type Germanium

U. S. Tandon and S. K. Kor

*Department of Physics, University of Allahabad, Allahabad 211002, India*

(Received 15 August 1972)

Attenuation suffered by compressional and shear acoustic waves propagating along the  $\langle 100 \rangle$  and  $\langle 110 \rangle$  directions has been evaluated from measured third-order elastic moduli for germanium metal in its pure and doped states at room temperature. The present results for pure germanium are in excellent agreement with previous attenuation measurements. As an effect of doping, an increase in phonon viscosity and in thermoelastic attenuation is observed. The resisting force acting against moving dislocations of both types is also presented.

### I. INTRODUCTION

The transfer of acoustic energy into thermal-phonon energy accounts for a major part of the acoustic-wave attenuation in crystals. Of the three

principal thermal causes<sup>1</sup> of ultrasonic attenuation in solids, only the phonon-viscosity mechanism and the thermoelastic phenomenon provides some non-negligible contributions for dielectric crystals.<sup>2</sup> In the former process, energy conversion